IMPROVEMENT IN STRENGTH CHARACTERISTICS OF CONSTRUCTION STEEL THROUGH INNOVATIVE COOLING

By

S.A. BALOGUN [1], G.I. LAWAL [2,] O.I. SEKUNOWO [3], S.O. ADEOSUN [4]
[1,2,3,4] Department of Metallurgical and Materials Engineering,
University of Lagos, Nigeria.

ABSTRACT

The increasing adverse effects of low strength characteristics of conventional hot rolled structural steel have become a major threat to safety of life and property. Several techniques aimed at achieving improved strength property of this class of steel include among others thermo-mechanical treatment, grain-size refinement, solid-solution hardening and precipitation hardening. However, the solid solution method is known to be the most suitable for improving strength properties of structural steels. Two processes, Tempcore and Thermex developed through solid solution hardening are plagued by some constraints that bother on patent restrictions, suitability for only integrated mill and a rather prohibitive cost. Most rolling plants in the third world countries are mini mills and hardly can afford the adoption of either process. In a bid to overcome some of these constraints and challenges, attempt is made in this study to develop a type of microstructure that enhances strength characteristics at a less drastic cooling rate through spray quenching. The method is cost effective, highly flexible and devoid of any need for plant re-engineering. Strength characteristics comparable with international standards specifications were achieved between 47 and 118 ^{o}C/s cooling rates within 15 seconds of spray quenching compared with about 500 ^{o}C/s conventional solid solution hardening practice.

Key words: *Strength characteristics, structural-steel, pearlite, lower bainite, spray-quenching*

1.0 INTRODUCTION

Several techniques aimed at achieving improved strength characteristics in metals and alloys have been employed in the past (Elmer et al, 1989; Centinel and Ozsoyeller, 2000; Sameer, et al, 2004; Bontcheva and Petzov, 2005). Some of these methods include thermo-mechanical treatment, grain-size refinement, solid solution hardening and precipitation hardening (Sinha, 1989). All these phenomena create substantial impediment to the motion of dislocation, which give rise to improved strength properties such as yield, tensile and impact toughness.

Ray, et al (1997) carried out a practical comparison of the strength developed through thermo-mechanical treatment (TMT) of plain carbon steel and copper bearing alloys. The quenching parameters were altered to achieve different yield strength levels. Both the plain carbon and alloyed steel grade TMT bars exhibited a composite microstructure consisting of ferrite-pearlite at the core and tempered martensite at the surface. The bars also conformed to strength requirements in the range 500-550 MPa with good elongation values (21-28%) and excellent bendability. This is an indication that plain carbon steel could be treated to develop strengths comparable to those of alloy steel grades.

Solid solution hardening principle was employed in the development of Tempcore and Thermex processes. Both processes were developed and patented in the mid-eighties to meet the challenge of low strength characteristics prevalent with conventional hot rolled mild steel bars (Markan, 2004). Tempcore process and its variant, Thermex process entail drastic cooling of hot rolled steel bar by immersion in a pool of water. The processes employ the principle of martensitic transformation through drastic cooling of hot rolled steel bars immediately after the finishing stand.

However, industrial transformation of austenite to martensite in mild steel requires a critical cooling rate up to 500 ^{0} C/s and must be accomplished within five seconds at most. This is often difficult to achieve. Thus, Tempcore and Thermex processes are fraught with two major constraints that have made their adoption difficult. One is the high cost of re-engineering of a typical conventional mill for Tempcore or Thermex

process technology. The other is the lack of information on process operating variables because of patent restrictions.

It is established (Dotrreppe, 2006) that without innovative hot rolling, steel bars produced through conventional route cannot exhibit adequate yield strength. One of the efficient and cost effective means of achieving improvement on the mechanical properties of conventional hot rolled steel bars may therefore, be found in developing a unique microstructure in which the grains play a major role.

Grain structure (size, shape and texture) is one of the primary characteristics that determine the mechanical properties of metals and their alloys [Henkel and Pense, 1977)]. This is predicated on the relationship that exists between grain-size and grain boundary on one hand and the interference of the latter with dislocation motion on the other (Curtin and Dewald, 2005). The interactions of dislocation with each other by slip and with surrounding crystal microstructures through cross-slip, glide and climb often result in enhanced strength in metals. Grain structures of varying sizes and morphology can be developed through a logical simulation of varying degrees of undercooling of steel bar from the austenitising temperature (Yada, 1987).

Microstructure of steel bars produced in conventional mill comprises ferrite and pearlite. This structure often confers considerable measure of plasticity with moderate strength and hardness (Samuel et al, 1990). Zambrano (2001) compared the microstructures of hot rolled bars from conventional and compact modern mils. Bars from the compact mill exhibited a dual-phase structure of martensite-pearlite. Differences in the mechanical behaviours of the bars were ascribed to the differences in their grain size coupled with variations in their textural components.

The formation of martensite however, requires drastic cooling rate, which is practically difficult to achieve in mild steel. Alternatively, a well controlled fast cooling of austenite could be effected such that lower bainitic microstructure is formed. This can be achieved through what can be described as a middle course critical cooling rate, which is between drastic quenching as obtained in martensitic hardening and air-cooling as obtained in conventional rolling

Lower bainitic structure forms in the temperature range 250^0-400^0C by a shear

transformation of austenite. The structure consists of ferrite solid solution saturated with carbon and particles of carbide occurring isothermally (Rollason, 1986).

Unlike in pearlite, the carbide particles in lower bainite are located within the plates of the α-phase due to the sluggish diffusion of carbon. This results in high dislocation densities in the bainite microstructure. Most polycrystalline materials contain dislocation density in the range 10^8 - $10^{12}cm^{-2}$ (Dieter, 1976). The carbide particles dispersed within the ferrite phase field act as barrier to the motion of dislocation, which enhances the bar's strength considerably (Schaffer et al, 1999). Bainite morphology varies with the type of carbide (Fe_3C , ε-carbide) based on transformation temperature and composition of steel (Honeycombe, 1982). Generally, lath martensite have similar structural characteristics with lower bainite, which has high dislocation densities around 10^{15}-$10^{16}cm^{-2}$ (Vijendra, 2004).

Development of lower bainitic structure in steel by this method constitutes a significant improvement on the conventional pearlitic structure. This is because lower bainite microstructure is known to confer enhanced strength property on the bar (Yu Lakthin, 1988).

The application of bainitic transformation (**BT**) is extensively used in the industry to strengthen critical structures and machine components. Lower bainitic steels (**LBS**) also, have widespread applications in structural members of bridges, cranes and other structures (Arvedi, et al, 2004). The high strength properties of LBS are due to the interstitial atoms of carbon and the high dislocation density in the α-martensitic phase (Henkel and Pence, 1977). Similarly, the formation of dispersed carbides in the-solid solution is also responsible for high hardness, strength and ductility of **LBS**.

In a bid to overcome some of the constraints and challenges prevalent with conventional mill practice, attempt is made in this study to develop lower bainite in preference to pearlitic structure in hot rolled mild steel bar. This will be accomplished through spray-quenching (SQ) of the bars on the cooling bed.

2.0 EXPERIMENTAL PROCEDURE

2.1 Material and Specimens

Hot rolled steel bar, **Nst 42/50HD** (AISI 1030, BS 970) was used to investigate the combined effect of varying austenitising

temperatures and cooling rates on microstructure and strength characteristics. A stock of the 12mm steel bars is shown in Figure 1 and the chemical composition including its carbon equivalent value (**Ceq**) is presented in Table 1.

Table 1: Chemical composition of the material used

St	ELEMENTS (%)												
ID	C	Si	S	P	Mn	Ni	Cr	Sn	Mo	V	Cu	Fe	*Ceq
G	0.231	0.250	0.055	0.034	0.602	0.102	0.120	0.034	0.020	0.002	0.274	98.276	0.38

$$*\mathbf{Ceq} = C + \frac{Mn}{6} + \frac{Cr + Mo + V}{5} + \frac{Ni + Cu}{15}$$

Where C, Mn, Cr, Mo, V, Ni and Cu are the chemical symbols for carbon, manganese, chromium, molybdenum, vanadium, nickel and copper respectively. The range of Ceq value (equation 2.1) obtained for each melt-cycle automatically places the steel in the class of weldable or non-weldable.

According to BS 4449: 1988 for weldable steel, Ceq $\leq$ 0.51 while Ceq $>$ 0.51 is for non-weldable steel. Table 2.3 is a compilation of the average chemical composition of billets used for high yield deformed bars by the Nigerian steel manufacturers. The concept of carbon equivalent Ceq, was introduced in order to control carbon concentrations to meet weldability criterion and strain hardening behaviour of rolling stocks. The weldability of steel is the ease with which it can be welded without complications or recourse to any special welding method.

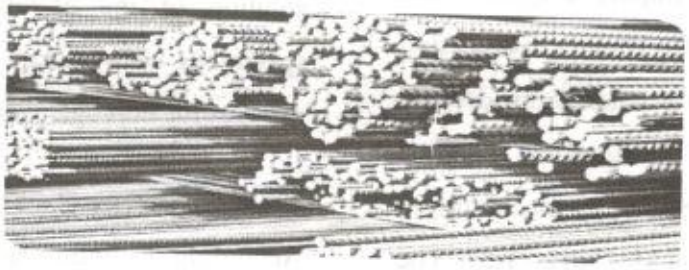

Figure 1: High yield hot rolled steel bars (12mm)

The most important set of mechanical property requirements in steel meant for structural applications under static loading are the tensile and hardness tests. Through tests, the steel, strength, stiffness, ductility and wear/abrasion resistance were

evaluated. These form the basic criteria for assessing the bar suitability under relevant service conditions.

Forty-nine (49) specimens for both hardness and tensile tests were prepared according to the British standard (**BS 18**) and the Nigerian Industrial Standards (**NIS 117-42/50HD 2004**). An **Instron** electro-mechanical tester **model 3369** operated at a cross head speed of 10mm/min. was used for the tensile tests. Specimen hardness values were evaluated using the **'B'** scale **Rockwell.**

Application of structural steel bars under dynamic loading such as bridges and buildings constructed along seismic prone areas are commonplace. Evaluation of the bar's susceptibility to brittle fracture under such conditions is imperative. Consequently, forty-nine charpy -v impact toughness test square specimens of 10x10mm cross-section and 50mm long with a notch 2mm deep at the middle of one of the sides and included angle of 45^0 were prepared by machining in accordance with **BS 131 (Parts 1-5).** The specimens were then subjected to impact loading using **Avery** impact tester (type 6703) at ambient temperature and a striking pendulum velocity of 5m/s. Energy absorbed at failure by each of the test specimens was read off from the scale.

2.2 Heat treatment

Test specimens were heated at the rate of 10^0C/min in a muffle furnace. The specimens, which are seven in each group are identified as A_1-A_7, B_1-B_7, C_1-C_7, D_1-D_7, E_1-E_7, F_1-F_7 and G_1-G_7 representing respectively the austenitising temperatures of 800^0, 820^0, 840^0, 860^0, 880^0, 900^0 and 1000^0C.This temperature range falls within and slightly above the intercritical ($\alpha + \gamma$) region of Fe-C equilibrium diagram on one hand and a simulation of typical hot rolling finishing temperatures on the other. This is aimed at eliminating the conventional α - pearlite structure in the bar and replacing it with α-austenite to facilitate efficient transformation on fast cooling. The α austenite structure is a homogenous solid solution of the as-rolled steel bar. The specimens were soaked between 10 and 15 minutes for homogenization.

2.3 Water-spray Cooling

According to industrial standard practice, 10,000litres/ton of water at ambient temperature is required to quench-harden plain carbon steel. This translates to 10litres/kg and 10ml/g water requirements

respectively. Approximately 0.321litres of water at ambient temperature is required to quench harden a 32.1g test specimen.

Therefore, the typical 12mm commercial steel bar weighing 10.658kg will require 106.6litres to quench harden it. Similarly, at an average production of 200tons/day, about two million litres of water will be needed at the cooling end. This volume of water is massive in view of the logistics that will be involved in its delivery and maintenance.

In this study, attempt was made to reduce the volume of water requirement by adopting pressurized spray quenching. Spray quenching under pressure enhances fast cooling as the formation of passive blanket film around specimen is prevented. Thus, 200ml of water was used in each spray-quench cycle of test specimens. This represents 37.7% reduction in water requirement daily. Spray quenching of specimens was carried out using a medium capacity, **0.5HP (0.37KW)** water pump. With appropriate variations in the piping-in and out of the pump, water flow rates **(ml/s)** of 40, 20, 13.3, 10, 8, 6.7 and 5 were achieved.

At the end of each cooling cycle, a digital pyrometer was used to obtain the temperature of test specimens. Figure 2 illustrates schematic diagrams of both the heat treatment and water-spray procedures.

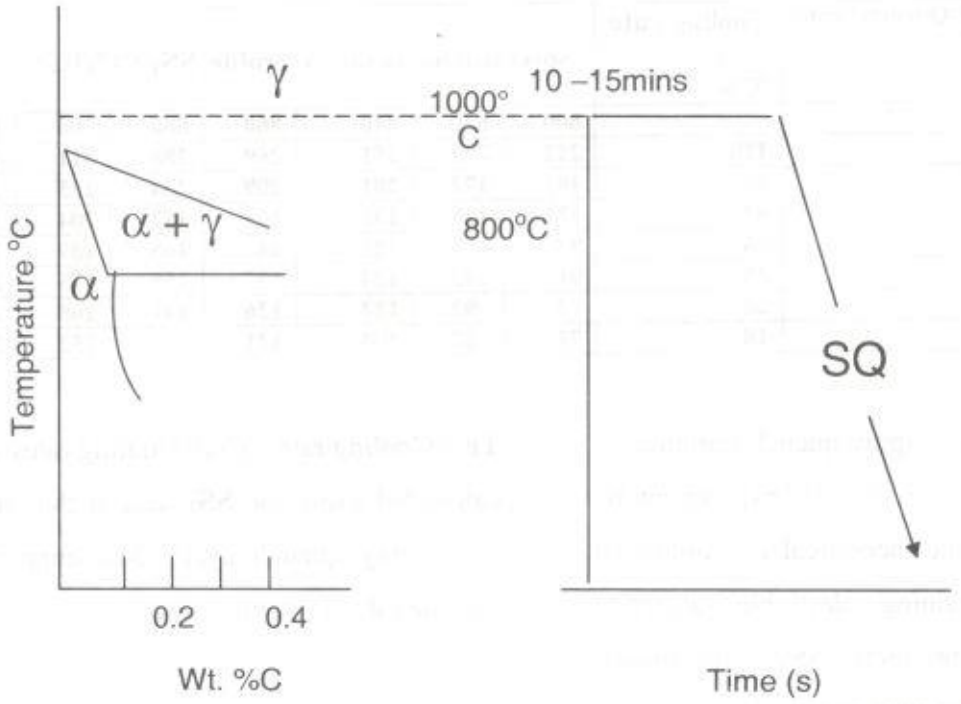

Figure 2: Schematic diagrams of heat treatment and spray-quench procedures.

2.4. Microstructural analysis

Direct correlations exist between a material's microstructure and its mechanical properties. It is therefore appropriate that the bars are subjected to microstuctural analysis. Test specimens (49) were prepared by polishing on a water-lubricated grinding machine using silicon carbide abrasive papers grades 240, 320, 400 and 600 grits. Final polishing of the specimens was effected with 0.5µm chromic oxide powders.

The surfaces so obtained were etched in 2% Nital solution, left for 30 seconds and then rinsed with water. The microstructural features of the specimens were examined under an inverted metallurgical microscope model **FEROX PL** at x 800 magnification.

Micrographs of the test specimens are presented on Plates 1-3 in Appendix A.

3.0 RESULTS AND DISCUSSION

3.1 RESULTS

3.1.1 Specimens temperature profile

The variations of measured temperatures of the spray-quenched specimens are presented in Table 2. The data are plotted in Figure 4. They are indicative of the specimens' degree of under cooling within the period stipulated in the experiment.

Table 2: Temperature profile of spray-quenched specimens

Time (SQ_d) S	Spray-Quench rate (SQ_r) ml/s	Cooling rate (T_r) ^{0}C/S	Specimen temperature profile, SS_T (^{0}C) 0.2%± 1°C						
			800	820	840	860	880	900	1000
5	40.0	118	212	233	251	269	288	311	410
10	20.0	65	165	172	201	209	234	255	352
15	13.3	47	113	121	135	168	182	204	301
20	10.0	36	98	102	128	143	168	189	282
25	8.0	28	91	113	124	137	155	176	272
30	6.0	24	73	92	112	126	141	168	267
40	5.0	18	71	87	104	121	136	152	253

Notations: SQ_d – Spray-quench duration(s): The SQ_d was preset for the experiment by synchronizing the theoretical and industrial time for obtaining desirable austenite decomposition products. SS_T – Specimens' temperature after quenching (^{0}C).

Tr – Cooling rate (^{0}C/s): Cooling rates were calculated using the SS_T data at the end of each spray quench cycle. Mathematically, cooling rate, **Tr** is given as;

$$Tr = \frac{Specimen\ austenitising\ temperature - Specimen\ temperature\ after\ quenching}{Spray\ quenching\ duration}$$

Thus,

$$Tr = \frac{A_T - SS_T}{SQ_d} \quad (^{o}C/s)$$

SQ_r – Spray-quench rate (ml/s): Varied volume of water flow was obtained by varying the piping dimensions in and out of the water pump during each quenching cycle.

3.1.2 Microstructural observation

Various microstructures were induced in the test specimens due to vaying cooling rates and austenitising temperatures, 800°C – 1000°C respectively while the specimens micrographs are shown on Plates 1-3.

3.1.3 Mechanical property

Tables 3 (a-g) in Appendix A are the computed true tensile strengths of test specimens from which flow curves displayed in Figures 3.1-3.7 are drawn. Tables 4.1-4.6 presented in Appendix B show the results of mechanical property of test specimens. Table 4.1 and Figure 8 were prepared in order to facilitate a quick comprehension of the yield strength exhibited by test specimens. The response to deformation under dynamic loading is shown in Tables 4.3 and 4.4 for air-cooled and spray-quenched specimens respectively. Hardness induced in test specimens at varying spray quenching rates and temperatures are presented in Table 4.6.

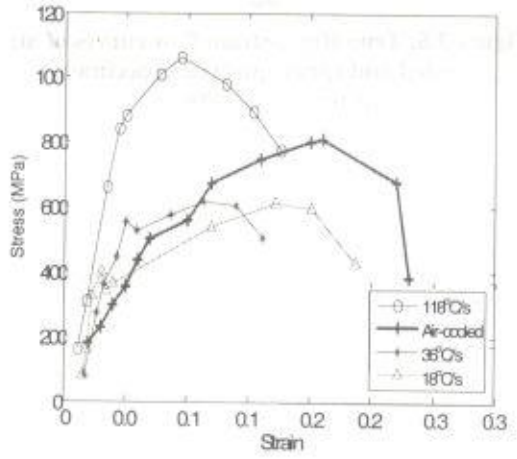

Figure 3.1: True stress-strain flow curves of air-cooled and spray-quenched specimen austenitised at 800° C

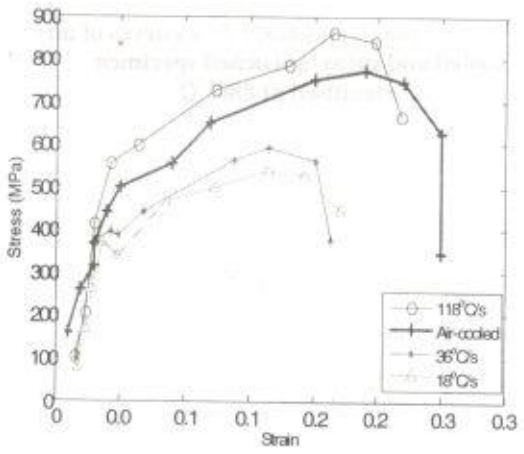

Figure 3.2: True stress-strain flow curves of air-cooled and spray-quenched specimen austenitised at 820°C

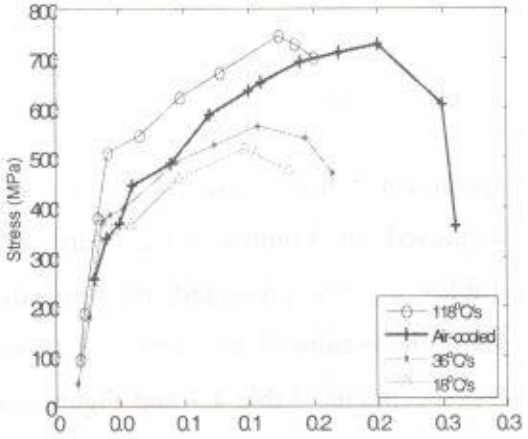

Figure 3.3: True stress-strain flow curves of air-cooled and spray-quenched specimen austenitised at 840° C

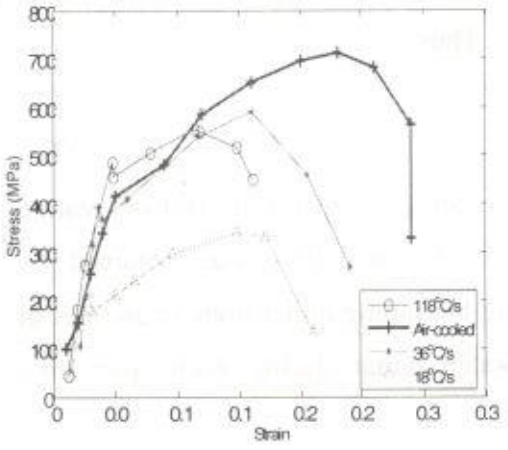

Figure 3.4: True stress-strain flow curves of air-cooled and spray-quenched specimen austenitised at 860° C

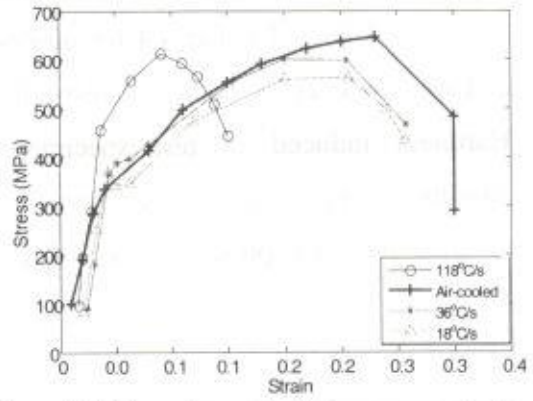

Figure 3.5: True stress-strain flow curves of air-cooled and spray-quenched specimen austenitised at 880° C

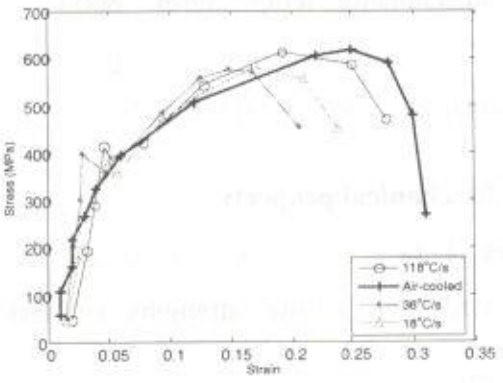

Figure 3.6: True stress-strain flow curves of air-cooled and spray-quenched specimen austenitised at 900° C

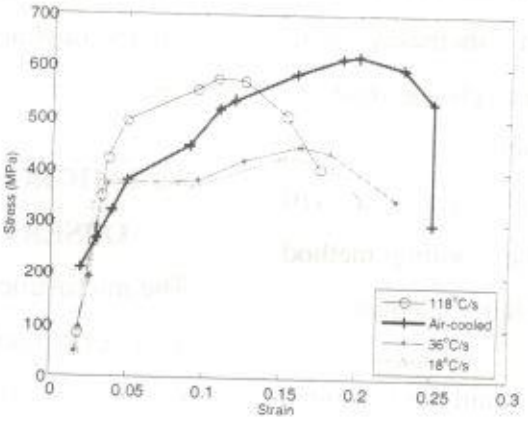

Figure 3.7: True stress-strain flow curves of air-cooled and spray-quenched specimen austenitised at 1000° C

3.2 DISCUSSION OF RESULTS

3.2.1 Evaluation of spray-quenching effectiveness

A relatively fast under cooling through varying water flow rates in contrast to the conventional air cooling of hot rolled steel bars led to changes in mechanical properties of the bars. This is expected (Vijendra, 1986) because, the greater the degree of under cooling of austenite the greater the propensity to transform.

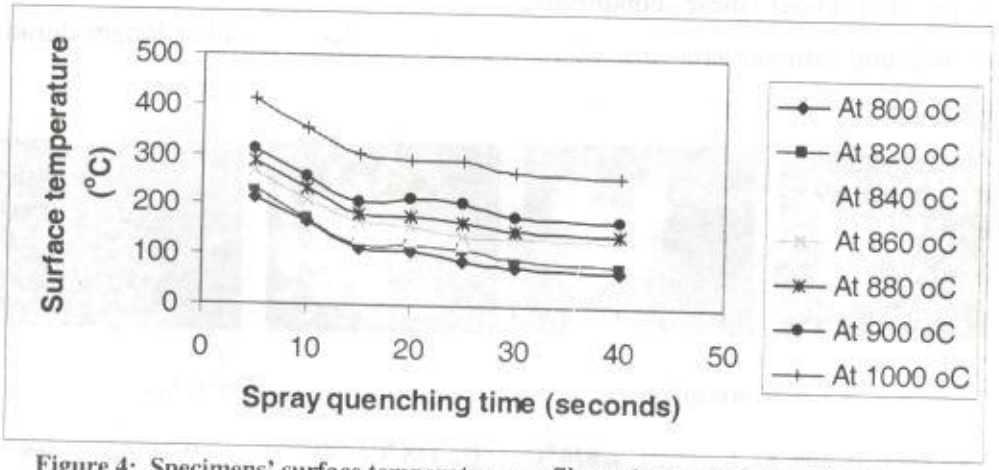

Figure 4: Specimens' surface temperature profile against spray quenching time

Figure 4 shows the variations in the test specimens' temperatures profile at the end of each spray-quenching cycle. Specimens' temperatures profile decreased down each of

the austenitising temperatures. This is due to time variations, which increases with successive cooling rates giving rise to additional cooling by natural effect. Given the observed temperature range of 71^0-410 ^{0}C, the efficiency of the cooling method adopted can be adjudged fairly adequate.

This temperature range would have resulted in the formation of a mixture of lower bainite and martensite on the surface and pearlite in the core of test specimens.

However, this was not the case with specimens austenitised between 880 ^{0} and 1000 ^{0}C and cooled in the range 24-18 ^{o}C/s.

This is due to the rather long duration (25-40 seconds) involved in cooling. Consequently, specimens treated under these conditions exhibited yield and ultimate strength values in the range of 633-842.8 MPa and 704.0 - 1173.6 MPa respectively. The hardness and impact toughness of the bars also improved considerably.

3.2.2.MICROSTRUCTURAL OBSERVATION

The microstructures developed in specimens after spray quenching at varying water flow rates are shown in Plates 1-3. The change in grain, shape and distribution are seen to depend on the specimens' temperature profiles after spray quenching. Grain sizes increased with decreasing cooling rates at each austenitising temperature. Lower bainite structure evolved in specimens having temperatures between 165^0 and 261^0C within 10min. of spray quenching. Similar low temperatures attained by other specimens could not induce lower bainitic phase due to a rather longer duration, 15-40 seconds of cooling.

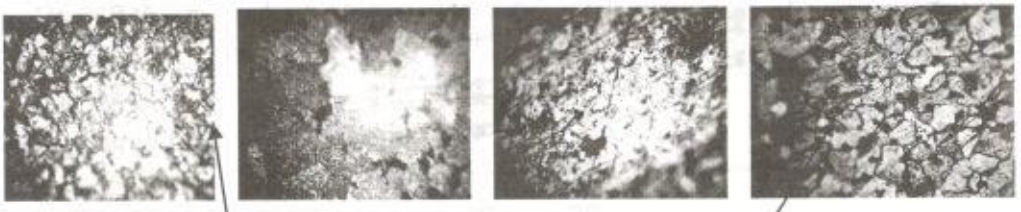

Carbide precipitates **Ferrite plate**

A_1, 118 ^{0}C/s, 800 ^{0}C **B_1, 118 ^{0}C/s, 820 ^{0}C** **C_1, 118 ^{0}C/s, 840 ^{0}C** **D_1, 118 ^{0}C/s, 860 ^{0}C**

A_2, 65 ^{0}C/s, 800 ^{0}C B_2, 65 ^{0}C/s, 820 ^{0}C C_2, 65 ^{0}C/s, 840 ^{0}C D_2, 65 ^{0}C/s, 860 ^{0}C

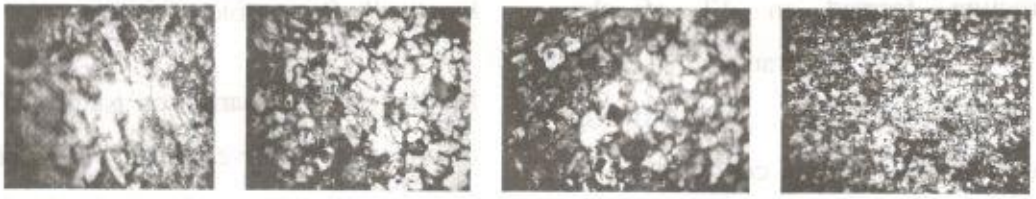

A_3, 47 ^{0}C/s, 800 ^{0}C B_3, 47 ^{0}C/s, 820 ^{0}C C_3, 47 ^{0}C/s, 840 ^{0}C D_3, 47 ^{0}C/s, 860 ^{0}C

PLATE 1: MICROGRAPHS OF TEST SPECIMENS SHOWING LOWER BAINITIC STRUCTURE (x800).

Micrographs on **Plate1** (A_1-A_3, B_1-B_3, C_1-C_3 and D_1-D_3) show lower bainitic microstructure formed in 12 of the specimens at the cooling range of 118-47 ^{0}C/s and 800^0-860^{0}C austenitising temperatures. The structure consists of lath carbide dispersed in a matrix of fine ferrite. Lath like bainite microstructure is similar to tempered martensite and is capable of exhibiting comparable mechanical properties (Ohtani, 2007). Fast under cooling of carbon steels from the austenitising temperature usually gives rise to decrease in the amount of proeutectoid phases present. This is because more carbon tends to precipitate out of solution thereby enriching the transformed portion in carbon.

This phenomenon occurs in a relatively short time for which such transformation is kinetically favourable.

Mixture of fine pearlite on islands of lower bainite was observed in 23 specimens as shown in **Plate 2** (A_4-A_5, B_4-B_5, C_4-C_5, D_4-D_5, E_1-E_5, F_1-F_5 and G_1-G_5). This transformation occurred within two different cooling ranges; that of 118-47 ^{0}C/s at 880^0-1000^{0}C and 36-28 ^{0}C/s between 800^0 and 1000^{0}C austenitising temperatures respectively. The combination of delayed transformation, 25 seconds, and a relatively low cooling rate are responsible for this transformation product.

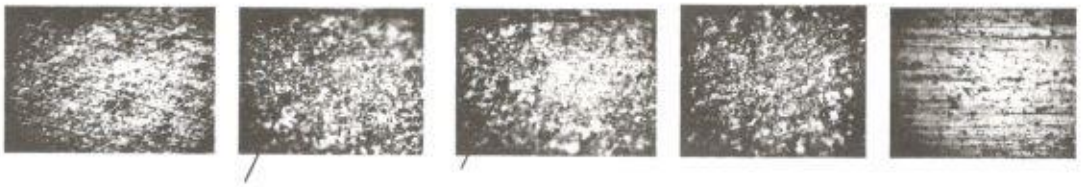

Fine cementite Fine ferrite

E_1, 118 ^{0}C/s, 880 ^{0}C F_1, 118 ^{0}C/s, 900 G_1, 118 ^{0}C/s, 1000 ^{0}C E_2, 65 ^{0}C/s, 880 ^{0}C F_2, 65 ^{0}C/s, 900^{0}C

G_2, 65 ^{0}C/s, 1000^{0}C E_3, 47 ^{0}C/s, 880^{0}C F_3, 47 ^{0}C/s, 900^{0}C G_3, 47 ^{0}C/s, 1000^{0}C A_4, 35 ^{0}C/s, 800 ^{0}C

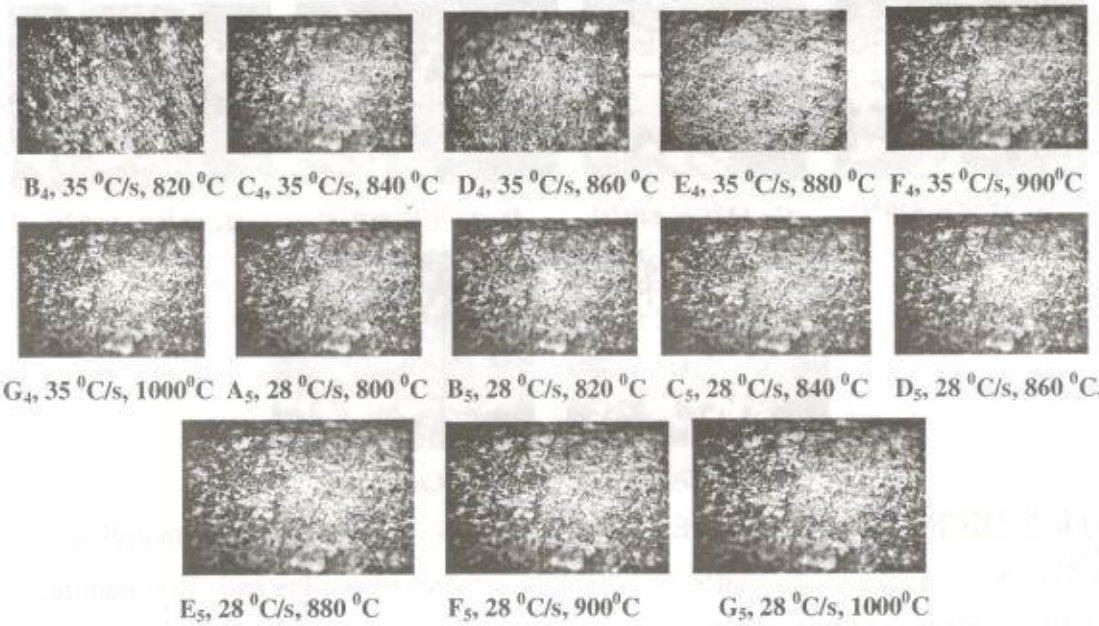

PLATE 2: MICROGRAPHS OF TEST SPECIMENS SHOWING FINE PEARLITIC STRUCTURE (x800).

Further decrease in cooling rate, 24-18 ^{0}C/s and longer duration of spray quenching gave rise to coarse pearlite at all austenitising temperatures. This is evident in the 14 micrographs on **Plate 3** (A_6-A_7, B_6-B_7, C_6-C_7, D_6-D_7, E_6-E_7, F_6-F_7 and G_6-G_7). Coarse pearlite degrades the specimens' hardness, yield strength, ductility and impact toughness. The foregoing microstructural observations are indicative of time and temperature dependence of austenite transformation in plain carbon steel.

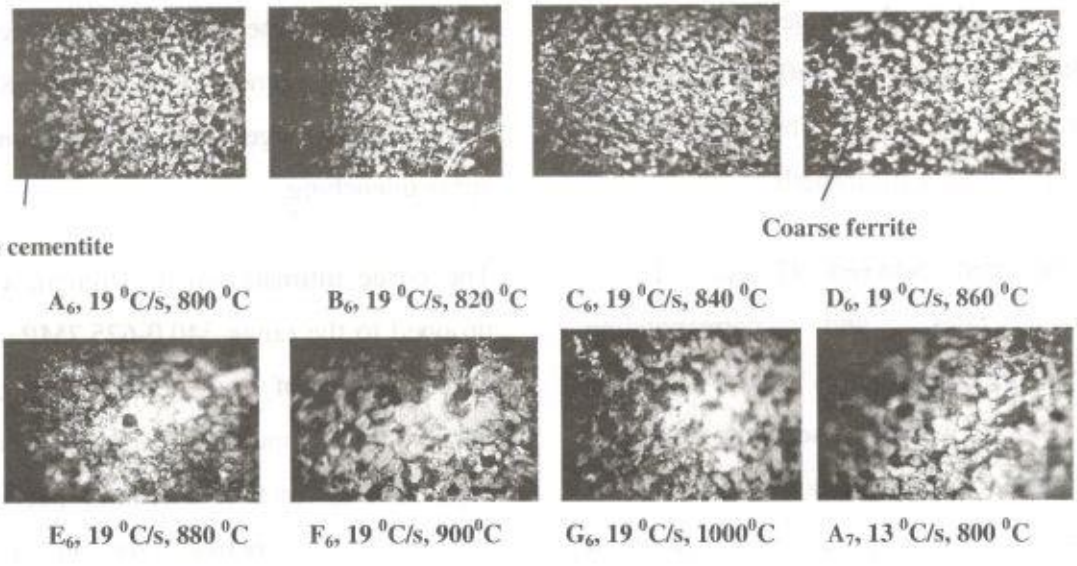

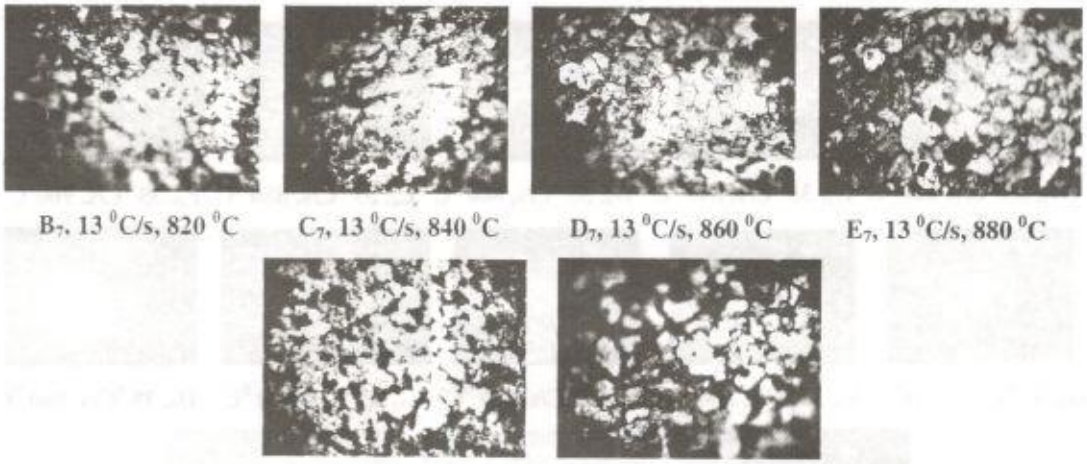

B_7, 13 ^{0}C/s, 820 ^{0}C C_7, 13 ^{0}C/s, 840 ^{0}C D_7, 13 ^{0}C/s, 860 ^{0}C E_7, 13 ^{0}C/s, 880 ^{0}C

F_7, 13 ^{0}C/s, 900^{0}C G_7, 13 ^{0}C/s, 1000^{0}C

PLATE 3: MICROGRAPHS OF TEST SPECIMENS SHOWING COARSE PEARLITIC STRUCTURE (x800).

3.2.3 Ultimate tensile strength

Figures 3.1-3.7 show the true stress-strain curves of air-cooled and spray-quenched test specimens. The curves indicate that the effect of increased cooling rates by spray quenching is quite significant. Spray-quenched specimens exhibited ultimate tensile strength in the range, 704-1173MPa compared with 616.7-806.9 MPa of conventional steel bar. This represents a mark-up of 31.9% in strength.

This occurred between 47 and 118^{0}C/s cooling rates and corresponding austenitising temperatures are in the range 800 ^{0}-860 ^{0}C within 15 seconds maximum spraying duration. Substantial increase in ultimate tensile strength can be explained in terms of the differing morphologies and textures of pearlite and lower bainite.

Pearlite is composed of alternate plates of ferrite and cementite with the thickness of the plate determining the grain size. In contrast, lower bainite comprised lath precipitates of carbide in ferrite matrix. The carbide precipitates act as barrier to dislocation motion hence, increase in ultimate tensile strength. However, sharp departure from the above was observed at higher heat treatment temperatures, 880 ^{0}-1000 ^{0}C, and longer time, 20-40 seconds of spray quenching.

The ensue ultimate tensile strength values dropped to the range 340.0-625.7MPa. This is indicative of the negative effect of delayed transformation of austenite whereby high volume fraction of coarse pearlite is formed. Worth noting however, is the

exceptionally high strength induced in the specimen at 800 ^{0}C within 47 and 118 ^{0}C/s cooling rates. This can be attributed to the high volume fraction of carbide precipitates formed under this condition.

3.2.4 Ductility

The amount of plastic strain suffered by the material before fracture corresponds to its ductility measured in percent elongation (%) at fracture. Good quality construction steel must possess appropriate level of ductility for an enhanced formability. All the test specimens exhibited adequate ductility having manifested this property in the range 15.0 -32.9% (Figure 5) compared with 28.2-41.9% in conventional bar. Again, the preponderance of carbide precipitates in the microstructure of is responsible for the marginal reduction in ductility.

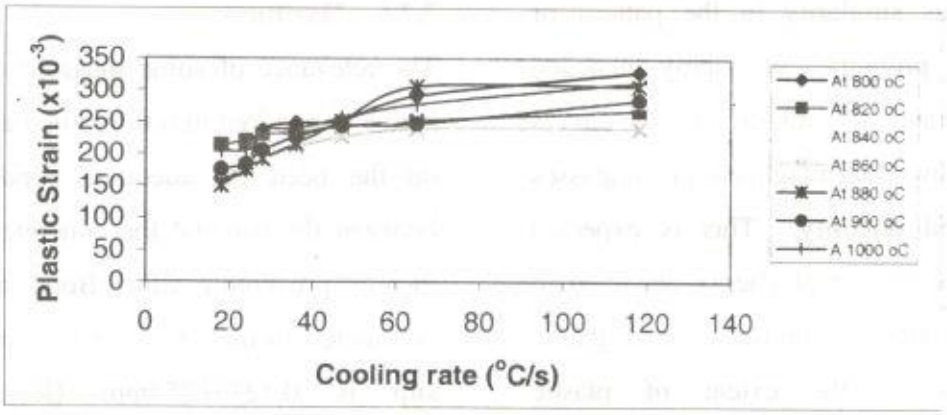

Figure 5: Plasticity properties of spray-quenched specimens at varying cooling rates

The minimum standard elongation for the steel bar under investigation is 10% of test specimen gauge length. It must be noted however, that beyond 35% elongation, the ductility becomes superfluous and the material is too soft to be used for reinforcement purposes.

3.2.5 Impact toughness

Sudden forces such as thunderstorms, seismic waves and irregular loading in the case of bridges, impact most structures.

Reinforcing steel bars are therefore required to possess adequate toughness under such conditions to prevent brittle failure. Figure 6 shows the impact toughness behaviours of test specimens.

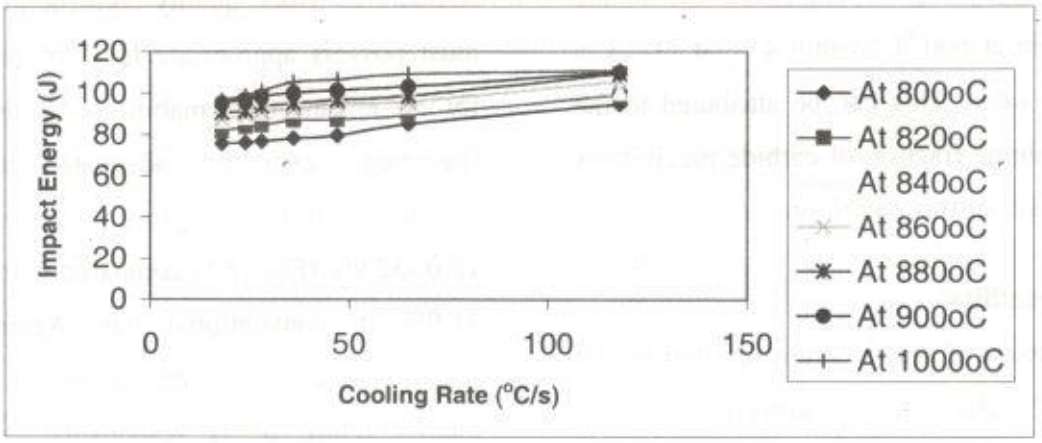

Figure 6: Impact toughness of spray-quenched specimens at varying cooling rates

The obvious similarity in the pattern of toughness property of spray-quenched specimens and the plastic strain curves (Figure) shows that toughness encompasses strength and ductility. This is expected because the amount of energy absorbed to break inter-atomic bonds between grains corresponds to the extent of plastic deformation suffered by test specimens. In the final analysis, spray quenched specimens exhibited higher impact toughness; 85.2-111.0 **J** compared with the as-rolled 78.4-82.0 **J** thereby adding value to the material.

3.2.6 Hardness

The relevance of some measure of surface hardness required in reinforcing bars bothers on the need for adequate bond strength between the bar and the concrete interface thereby preventing slip. Bond strength is considered to have failed when the relative slip is 0.127-0.254mm (Rao, 1961). Occurrence of slip usually gives rise to the failure in the adhesion between the reinforcement and the concrete interface. The bars ribs must therefore exhibit sufficient wear resistance in order to function effectively

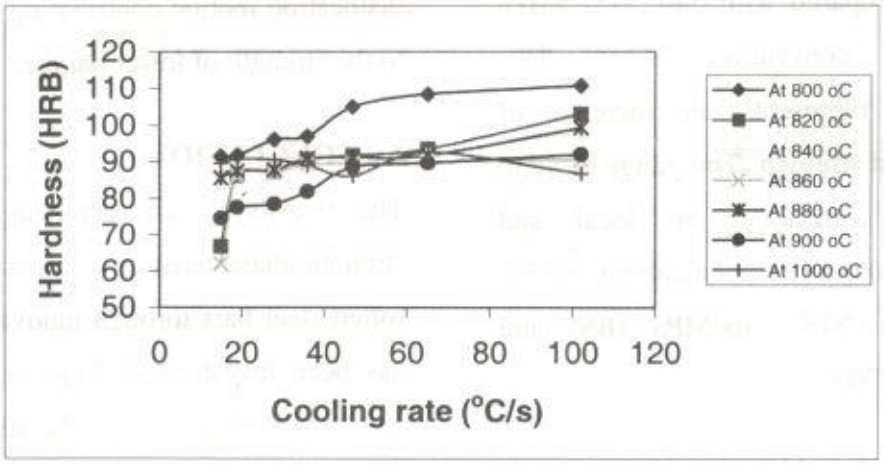

Figure 7: Hardness of spray-quenched specimens at varying cooling rates.

Specimens at all austenitisation temperatures but within 47 and 118 ^{0}C/s cooling rates show increased hardness (Figure 7) in the range of 84.3-110.8 **HRB** compared with that obtained in conventional bar, 62.1-93.7**HRB.** The hardness level exhibited by the spray-quenched specimens further confirms that lower bainite share some microstructural similarities with tempered martensite.

3.2.7 Yield strength

Yielding of ductile material such as steel produces permanent deformation (Kempter, 1979). Hence, yield strength is an important design parameter in engineering.

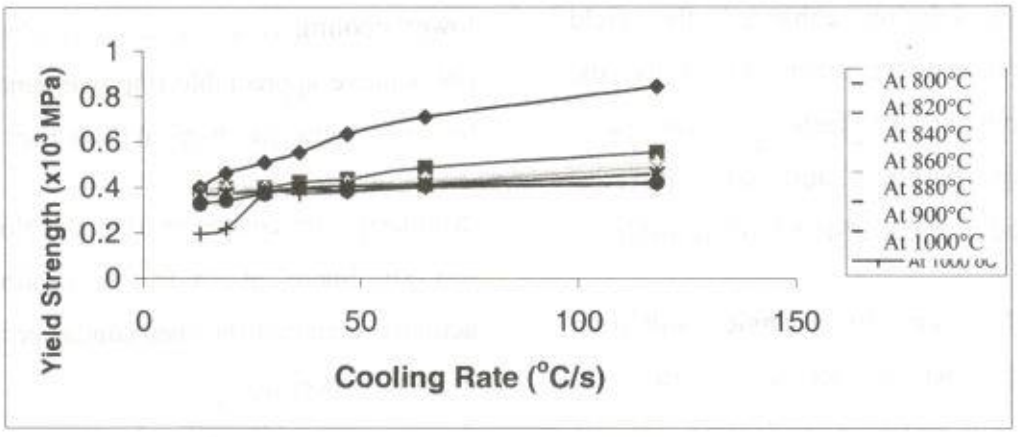

Figure 8: Yield strength properties against cooling rate

From Figure 8, it is observed that specimens subjected to cooling in the range 47-118 ^{0}C/s of 800^0-880^{0}C treatment temperatures exhibited yield strength in the range 421.9-

842.8MPa compared with 340.1-452.8MPa obtained in conventional bars. This development represents an increase of 59.5% in yield strength. This range of yield strength is comparable to local and international standard specifications, which are 420MPa (**NIS**), 460MPa (**BS**) and 500MPa (**ASTM**).

The concept of yield in low carbon steels depends heavily on the presence of small interstitial atoms such as carbon, boron, and nitrogen. The amount and distribution of any of these interstitial atoms govern the yield behaviour of the material (Hall, 1970).

Increase in yield property of test specimens can therefore be explained in term of the texture of lower bainite. Carbide precipitates act as interstitial elements in addition to the carbon in solution enhanced the yield strength of test specimens. Generally, the yield strength of steels increases with decreasing bainite lath size just as established by the Hall-Petch relationship.

The laths are low angle sub-grain boundaries, which act as barriers to dislocation motion contributing significantly to the strength of lower bainite.

4.0 CONCLUSION

The feasibility of achieving improved strength characteristics in constructional hot rolled steel bars through innovative cooling has been investigated. Improvement in the mechanical properties of the steel bars was achieved in the cooing range 118-47 ^{0}C/s and 800^0-860^{0}C finishing temperatures within 5-15 seconds water spray quenching.

The development of lower bainitic microstructure in 12 of the specimens led to increase by 39%, 45% and 22% respectively in yield strength, ultimate tensile strength and impact toughness but 9% decrease in ductility compared to the conventional steel bar. Due to delayed transformation, the lower cooling range, i.e., 36-28^{0}C/s could not achieve appreciable improvement in the test specimens' mechanical properties.

Similarly, the coarse pearlite developed in test specimens at 24-18^{0}C/s cooling rate actually impaired the mechanical properties of 14 test specimens.

APPENDIX A: TRUE STRESS-STRAIN DATA OF SPRAY-QUENCHED SPECIMENS AT VARYING AUSTENITISING TEMPERATURES

Table 3a: True stress-strain at 800 ^{O}C

Water-spray duration (s)													
5		10		15		20		25		30		40	
Strain	Stress	Strain	Stress	Strain	Stress	Strain	Stress	Strain	Stress	Strain	Stress	Strain	Stress
0.012	161.1	0.026	159.3	0.014	134.7	0.017	80.4	0.070	107.6	0.027	147.9	0.016	80.9
0.019	308.3	0.047	638.7	0.018	257.8	0.027	271.0	0.083	326.6	0.032	262.1	0.019	162.3
0.035	661.9	0.050	709.9	00.026	406.0	0.033	361.8	0.092	494.4	0.044	405.9	0.023	325.8
0.045	842.8	0.063	685.5	0.031	509.0	0.043	446.0	0.093	508.3	0.050	461.0	0.031	398.3
0.050	884.5	0.069	748.4	0.040	633.0	0.050	553.0	0.117	490.8	0.055	435.0	0.034	340.3
0.078	1008.2	0.135	1015.0	0.079	687.7	0.059	524.9	0.131	560.8	0.089	509.7	0.040	360.5
0.095	1061.7	0.176	1110.6	0.110	796.4	0.087	576.3	0.191	693.1	0.135	627.6	0.120	538.9
0.131	981.2	0.218	1173.6	0.153	8887.3	0.113	614.4	0.218	732.2	0.205	704.0	0.172	614.1
0.154	893.1	0.305	1158.9	0.191	939.2	0.140	604.5	0.247	724.1	0.255	694.2	0.201	596.9
0.176	775.4	0.329	1015.4	0.248	825.6	0.162	505.9	0.252	506.8	0.291	556.1	0.237	427.1

Table 3b: True stress-strain at 820 ^{0}C

Water-spray duration (s)													
5		10		15		20			25	30		40	
Strain	Stress	Strain	Stress	Strain	Stress	Strain	Stress	Strain	Stress	Strain	Stress	Strain	Stress
0.016	101.9	0.018	51.7	0.018	50.2	0.017	95.8	0.019	46.9	0.016	49.2	0.018	75.1
0.024	205.3	0.023	207.7	0.029	217.0	0.027	290.2	0.024	188.5	0.020	148.1	0.024	166.9
0.030	413.0	0.032	311.9	00.31	305.30	0.033	377.9	0.031	284.7	0.022	194.9	0.029	260.9
0.043	554.7	0.044	435.1	0.039	410.7	0.043	395.4	0.036	381.8	0.026	183.7	0.037	369.5
0.064	598.5	0.068	407.1	0.044	397.2	0.049	384.8	0.041	352.0	0.043	227.4	0.048	335.6
0.124	726.3	0.136	438.9	0.070	436.5	0.068	441.0	0.060	372.4	0.091	304.2	0.085	464.2
0.180	784.8	0.194	586.0	0.134	569.2	0.138	565.1	0.107	500.9	0.147	348.6	0.123	499.6
0.215	862.4	0.228	638.7	0.179	607.7	0.165	591.70	0.172	555.9	0.169	363.9	0.164	540.1
0.247	840.5	0.262	619.5	0.195	602.7	0.201	560.1	0.203	545.2	0.204	356.1	0.192	525.7
0.268	664.9	0.252	346.30	0.242	456.6	0.213	377.7	0.230	457.3	0.233	248.0	0.220	442.5

Table 3c: True stress-strain at 840 ^{0}C

Water-spray duration (s)													
5		10		15		20			25	30		40	
Strain	Stress	Strain	Stress	Strain	Stress	Strain	Stress	Strain	Stress	Strain	Stress	Strain	Stress
0.019	93.40	0.016	44.4	0.019	44.8	0.017	44.6	0.018	95.1	0.019	96.4	0.019	82.7
0.022	187.4	0.024	178.9	0.022	89.9	0.026	179.9	0.025	191.6	0.026	194.0	0.029	250.7
0.033	379.3	0.037	362.6	00.31	113.4	0.037	373.2	0.031	376.1	0.031	383.2	0.033	335.9
0.041	508.8	0.043	405.70	0.036	182.5	0.042	384.1	0.040	389.20	0.049	387.2	0.036	373.7
0.066	543.5	0.051	382.2	0.052	389.1	0.054	398.1	0.062	407.7	0.095	488.9	0.045	354.6
0.97	622.5	0.174	442.1	0.067	404.5	0.094	490.5	0.093	492.1	0.154	562.8	0.059	364.0
0.128	670.9	0.142	553.8	0.078	386.2	0.124	526.0	0.149	564.5	0.169	584.3	0.096	456.9
0.174	743.2	0.173	589.7	0.140	536.3	0.158	563.8	0.177	541.2	0.183	574.1	0.147	516.1
0.186	727.6	0.207	454.6	0.212	617.3	0.194	538.6	0.183	534.3	0.210	565.9	0.156	507.8
0.200	699.4	0.256	465.6	0.284	453.60	0.215	467.4	0.191	466.1	0.228	476.9	0.181	473.7

Table 3d: True stress-strain at 860 ^{0}C

Water-spray duration (s)													
5		10		15		20			25	30		40	
Strain	Stress	Strain	Stress	Strain	Stress	Strain	Stress	Strain	Stress	Strain	Stress	Strain	Stress
0.012	45.1	0.020	95.0	0.022	97.4	0.021	104.0	0.017	101.3	0.021	86.6	0.014	48.9
0.019	182.0	0.022	190.3	0.028	195.9	0.026	209.1	0.019	202.0	0.031	349.8	0.019	147.3
0.025	274.7	0.037	286.9	00.35	296.1	0.032	315.7	0.027	305.4	0.037	394.4	0.029	218.2
0.048	487.0	0.037	422.4	0.045	41.7	0.037	394.5	0.032	394.2	0.045	368.2	0.031	178.3
0.049	457.7	0.038	387.0	0.053	391.7	0.040	365.9	0.039	372.1	0.056	403.8	0.050	212.7
0.079	507.4	0.65	436.7	0.080	441.1	0.060	411.2	0.065	417.7	0.066	416.7	0.066	241.9
0.114	556.2	0.119	534.7	0.117	542.5	0.117	538.2	0.095	485.1	0.128	529.9	0.096	297.1
0.118	550.7	0.141	576.7	0.162	592.1	0.160	590.1	0.130	535.2	0.166	586.2	0.148	340.0
0.148	518.5	0.153	551.6	0.188	577.9	0.205	268.8	0.155	531.9	0.186	579.5	0.171	332.1
0.161	451.40	0.191	493.7	0.239	471.0	0.240	459.1	0.180	431.5	0.226	463.2	0.210	132.4

Table 3e: True stress-strain at 880 ^{0}C

Water-spray duration (s)													
5		10		15		20			25	30		40	
Strain	Stress	Strain	Stress	Strain	Stress	Strain	Stress	Strain	Stress	Strain	Stress	Strain	Stress
0.016	97.6	0.027	95.6	0.019	107.2	0.024	89.8	0.017	96.5	0.018	99.7	0.021	82.9
0.020	195.9	0.031	192.0	0.027	216.1	0.031	180.8	0.023	194.2	0.022	200.2	0.033	251.9
0.028	291.1	0.037	289.9	00.38	421.9	0.044	366.5	0.033	357.9	0.028	302.1	0.044	370.5
0.036	458.0	0.041	388.1	0.040	383.3	0.051	387.4	0.049	350.8	0.034	324.4	0.051	341.7
0.064	557.8	0.045	487.0	0.065	421.0	0.062	397.0	0.054	390.9	0.041	379.3	0.063	347.6
0.91	613.5	0.065	556.4	0.095	497.6	0.080	427.3	0.057	357.4	0.043	358.9	0.119	473.2
0.109	593.1	0.096	645.8	0.154	577.1	0.154	555.1	0.131	534.0	0.065	397.1	0.200	559.7
0.123	564.7	0.161	763.3	0.176	605.5	0.200	601.8	0.162	559.6	0.138	535.8	0.257	561.7
0.138	509.0	0.176	756.5	0.210	591.4	0.255	599.5	0.190	550.8	0.155	514.8	0.289	501.4
0.150	444.7	0.192	628.2	0.251	405.1	0.307	467.0	0.215	466.2	0.175	302.9	0.306	436.2

Table 3f: True stress-strain at 900 ^{0}C

Water-spray duration (s)													
S		10		15		20			25	30		40	
Strain	Stress	Strain	Stress	Strain	Stress	Strain	Stress	Strain	Stress	Strain	Stress	Strain	Stress
0.018	85.7	0.014	45.8	0.017	47.3	0.017	47.3	0.017	45.9	0.017	42.6	0.017	45.4
0.028	259.7	0.019	92.1	0.019	94.9	0.019	94.9	0.022	135.5	0.023	86. 1	0.019	19.0
0.033	348.3	0.022	184.6	00.23	190.5	0.026	191.1	0.025	230.8	0.025	172. 6	0.023	182.8
0.037	419.6	0.027	278.3	0.0373	384.4	0.030	287.7	0.037	370.1	0.035	340. 5	0.025	228.9
0.049	495.2	0.048	411.4	0.050	362.1	0.037	372.0	0.067	294.50	0.066	356. 1	0.027	326.5
0.095	556.7	0.051	389.2	0.082	454.6	0.096	378.8	0.129	429.1	0.096	417. 2	0.032	381.4
0.108	575.2	0.067	444.20	0.128	529.3	0.126	419.20	0.194	457.8	0.127	473. 6	0.095	368.5
0.126	572.0	0.129	587.0	0.183	583.7	0.163	447.30	0.216	456.80	0148	493. 0	0.152	427.3
0.154	506.1	0.166	630.7	0.214	583.2	0.183	434.8	0.256	434.80	0.156	492. 7	0.182	412. 7
0.176	407.1	0.247	489.0	0.244	472.6	0.226	344.9	0.285	344.9	0.184	443. 3	0.205	341. 0

Table 3g: True stress-strain at 1000 ^{0}C

Water-spray duration (s)													
5		10		15		20			25	30		40	
Strain	Stress	Strain	Stress	Strain	Stress	Strain	Stress	Strain	Stress	Strain	Stress	Strain	Stress
0.020	47.5	0.024	86.9	0.018	93.4	0.015	49.9	0.019	45.2	0.016	42.5	0.015	42.7
0.032	192.4	0.030	174.7	0.024	187.9	0.021	200.8	0.026	181.9	0.023	171.0	0.025	172.6
0.038	290.2	0.034	263.4	0.029	283.1	0.027	302.9	0.038	276.3	0.030	258.5	0.028	259.7
0.046	414.9	0.043	398.0	0.033	379.3	0.029	398.5	0.047	376.3	0.037	369.9	0.048	368.2
0.053	385.2	0.059	369.0	0.0050	378.3	0.049	356.2	0.067	375.3	0.040	349.8	0.057	356.7
0.079	423.1	0.115	523.4	0.066	401.1	0.094	486.3	0.120	529.5	0.079	452.2	0.095	472.4
0.128	542.6	0.151	582.0	0.097	493.1	0.125	557.0	0.165	597.0	0.116	515.3	0.126	525.2
0.192	613.70	0.205	626.7	0.146	545.90	0.148	575.3	0.192	588.8	0175	589.4	0.170	583.0
0.250	585.80	0.251	579.8	0.157	544.0	0.167	569.5	0.209	560.2	0.220	572.2	0.210	555.9
0.278	472.3	0.313	483.8	0.205	423.2	0.206	455.1	0.237	460.4	0.256	357.4	0.239	449.3

APPENDIX B: MECHANICAL PROPERTY DATA OF SPRAY-QUENCHED STEEL

Table 4.1: Yield strength property of test specimens

Chorus: Ye heavenly Host, rejoice with usCooling rate ^{0}C/s	Yield Strength (MPa)/Temperature (^{0}C)						
	800	820	840	860	880	900	1000
118	842.8	554.2	508.8	487.0	458.0	419.6	414.9
65	709.9	487.0	435.1	422.4	411.4	405.7	398.0
47	633.0	425.7	417.3	410.7	404.5	384.4	379.3
36	553.0	421.9	398.5	398.1	395.4	394.5	372.0
28	508.3	397.0	394.2	389.2	381.8	371.6	370.1
24	461.0	394.4	390.9	382.2	369.9	340.5	218.2
8	398.3	379.3	373.7	369.5	368.2	326.5	194.9

109

Table 4.2: stiffness variations of test specimens

Cooling rate ^{0}C/S	Modulus (MPa)/ Temperature (^{0}C)						
	800	820	840	860	880	900	1000
118	18321.7	12606.8	12095.2	9938.8	12378.4	11042.1	8827.7
65	13919.6	11156.4	9220.5	11115.8	10587.0	10034.1	9045.5
47	15439.0	10267.5	5862.3	9080.4	10817.9	10115.8	11155.9
36	10843.1	8936.4	7108.9	10302.6	6203.7	9789.5	13741.4
28	5186.7	10318.9	9492.7	11945.5	6980.4	9739.5	7839.6
24	9039.2	8859.1	12361.1	10378.9	9031.0	9458.3	9734.2
18	6623.1	9723.7	10100.0	7524.1	8233.3	12092.6	8980.5

Table 4.3: Impact energy of air-cooled (as-rolled) test specimens

Specimen number	1	2	3	4	5	6	7
Impact energy (J)	81.9	80.7	81.5	82.0	78.4	79.6	80.3

Table 4.4: Impact energy absorbed at varying cooling rates and temperature by test specimens

Cooling rate ^{0}C/S	Impact energy (J) / Temperature (^{0}C)						
	800	820	840	860	880	900	1000
118	94.8	99.1	100.2	105.7	109.3	110.0	111.0
65	85.2	89.4	93.7	96.0	98.7	103.2	109.2
47	79.6	87.2	92.6	94.9	96.8	101.4	106.5
36	78.3	86.9	91.7	92.5	95.1	100.2	105.4
28	76.9	84.6	90.4	91.2	93.7	98.6	101.2
24	76.2	83.8	88.5	89.3	91.4	97.1	98.7
18	75.7	81.7	86.8	87.6	90.5	95.3	96.8

Table 4.5: Plastic strain variations of test specimens

Cooling rate ^{0}C/S	Strain (x 10^{-3}) Temperature (^{0}C)						
	800	820	840	860	880	900	1000
118	176	268	200	161	150	176	278
65	329	262	256	191	192	247	313
47	248	242	282	239	251	244	205
36	162	213	215	240	307	226	206
28	252	230	191	180	215	285	237
24	291	233	228	226	175	184	256
18	237	220	181	210	306	205	239

Table 4.6: Hardness of spray-quenched test specimens

Cooling rate ^{0}C/S	Hardness value (HRB)/ Temperature (^{0}C)						
	800	820	840	860	880	900	1000
118	108.5	103.1	98.3	87.1	91.4	88.6	86.8
65	110.8	93.6	90.5	89.4	99.3	92.1	92.7
47	105.1	91.8	92.3	90.0	91.0	89.8	86.2
36	91.6	90.7	87.4	90.6	91.8	77.6	89.1
28	97.0	87.4	88.3	86.1	87.9	78.5	90.6
24	96.2	86.8	89.1	89.6	85.7	81.9	90.8
18	91.8	86.2	84.3	62.0	87.6	74.6	89.7

REFERENCES

1. Arvedi, G. and Guindani, A. (2004), "Metallurgical Based Development of Dual Phase Thin Hot Strip.", Acciaiena Arvedi S.P.A., Ceremona, Italy, pp.1-2.

2. Bontcheva, N. and Petzov, G. (2005), "Total Simulation Model of the thermo-mechanical process in shape rolling of steel rods.", Journal of Computational Materials Science, vol.34, Issue4, December, 2005, pp. 377-388.

3. Centinel Ozsoyeller (2000), "A finite element based prediction of microstructural evolution of steels subjected to Tempcore process.", Journal of Mechanics of Materials, vol.32, Issue 6, June 2000, pp. 339-347.

4. Curtin, W. A. and Dewald, M. (2005), "Multiscale Modeling of Dislocation/Grain Boundary interactions", Session V34, Multiscale phenomenona for Fluid and Solid. March, 2005, 520A.

5. Dieter, E. George (1988), "Mechanical Metallurgy", McGraw-Hill Book Company, SI Metric Edition, pp. 145-240.

6. Dotreppe, J. C. (2006), "Mechanical Properties of Quenched and Self-Tempered Reinforcing Steel at Elevated Temperatures compared with Recommendations of Eurocode 2, part 1-2", Journal of Materials and Structures, vol. 30, No. 7, October, 2006, pp. 430-438.

7. Elmer, J. W., Allen, S. M. and Eagar, T. W. (1989), " Microstructural Development during solidification", Metallurgical Transactions A, Vol. 20A, No. 10, October, 1989, pp. 2117-2131.

8. Hall, E. O. (1970), "Yield Point Phenomenon in metals", Plenum Publishing Company, New 2nd Edition, York, pp.49-72.

9. Henkel and Pense (1977), "Structure and Properties of Engineering Materials", McGraw-Hill Series in Materials Science, 5th Edition, pp. 189-191.

10. Honeycombe, R. W. K. (1982), "Steels Microstructure and Properties", Edward Arnold Limited, London, 2nd Edition, pp. 31-78.

11. Kempter, M. H. A. (1979), "Materials for Engineers", Hodder and Stoughton

Publishers, London, 3rd Edition, pp. 48-61.

12. Markan, R. K. (2007), "Thermex QST Rebars", Thermex Quenching and Tempering Technology, September, 2007, pp. 4-11.

13. Ohtani, H., Okaguchi, S., Fujishiro, Y. and Ohmori, Y. (2007), "Morphology and properties of low-carbon bainite", Metallurgical and Materials Transactions A, Vol. 21, No. 3, March, 2007, pp. 877-888.

14. Rao, K. L. (1961), "Calculation, Design and Testing of Reinforced Concrete", Isaac Pitman and Sons Limited, London, p. 97.

15. Ray, A., Mukerjei, D., Sen, S. K., Bhaltcharya,A., Dhua, S. K., Prasad, M. S., Barnerjie, N., Ppli, A. M. and Sahu, A. K. (1997), "Microstructure and Properties thermomechanically strengthened reinforcement bars: a comparative assessment of plain-carbon and low-alloy steel grades", Journal of Materials Engineering and Performance, Vol.6, No.3, June, 1997, pp. 335-343.

16. Rollason, E. C. (1973), "Metallurgy for Engineers", Edward Arnold Publishers, London, 4th Edition, pp. 121-128.

17. Sameer Phadke, Praveen Pauskar, and Rajiv Shivpuri (2004), "Computational Modeling of Phase Transformation and Mechanical Properties During the Cooling of Hot Rolled Rod", Journal of Materials Processing Technology, Vol. 150, Issue 1-2, July 2004, pp. 107-115.

18. Sinha, A. K. (1989), "Ferrous Physical Metallurgy", Butherworth Publishers, London, p. 56.

19. Vijendra Singh (2004), "Heat Treatment of Metals", Standard Publishers, New Delhi, 2nd Edition, pp. 94-153.

20. Yada, H. (1987), "Accelerated cooling of rolled steel", The Metallurgical Society, CIMM, Wimnipeg, MB Canada, pp. 105-120.

21. Yu M. Lckhtin (1983), "Engineering Physical Metallurgy and Heat Treatment", Mir Publishers, Moscow, 2nd Edition, pp. 184-224.

22. Zambrano, P. C., Guerrero, M. P., Colas, R. and Ledue, L. A. (2001), "Microstructural analysis of hot-rolled low-carbon steel strips", Journal of

Materials Characterisation, Vol. 47,

Issue 3-4, November, 2001, pp. 275-282.